AGU PUBLICATIONS

Geophysical Research Letters

RESEARCH LETTER
10.1002/2015GL064806

Key Points:
- Breaking the magnetotail symmetry increases possibility of substorm triggering
- Extension of the existing Vlasov equation solutions for the bent current sheet
- Possible reason of substorm occurrence coupling with solar wind direction jumps

Correspondence to:
V. S. Semenov,
sem.geo.phys@spbu.ru

Citation:
Semenov, V. S., D. I. Kubyshkina, M. V. Kubyshkina, I. V. Kubyshkin, and N. Partamies (2015), On the correlation between the fast solar wind flow changes and substorm occurrence, *Geophys. Res. Lett.*, *42*, 5117–5124, doi:10.1002/2015GL064806.

Received 3 JUN 2015
Accepted 16 JUN 2015
Accepted article online 18 JUN 2015
Published online 14 JUL 2015

On the correlation between the fast solar wind flow changes and substorm occurrence

V. S. Semenov[1], D. I. Kubyshkina[1], M. V. Kubyshkina[1], I. V. Kubyshkin[1], and N. Partamies[2,3]

[1]Earth Physics Department, Saint Petersburg State University, Saint Petersburg, Russia, [2]Finnish Meteorological Institute, Helsinki, Finland, [3]Currently at Middle Atmospherics Physics, University Centre in Svalbard, Longyearbyen, Norway

Abstract There is a point of view that solar wind factors, which break the magnetotail symmetry, are more effective in triggering the magnetospheric substorm. To clarify the question we use a database of substorm onsets and found the evident dependence of the substorm probability on the solar wind flow direction jumps (asymmetric factor), while distribution of the substorm occurrence on the solar wind number density jumps (symmetric factor) is homogeneous. The theoretical interpretation is based on the extension of the existing symmetric Kan model for a bent current sheet. Allowing the model tilt angle to vary in time, we found that the induced electric field penetrates to the central region of the bent current sheet. If the solar wind direction jump increases the bending, then induced electric field thins the current sheet and thus stimulates the reconnection. In the opposite case the current sheet thickens. We claim that this effect is sufficient (provides twice or more thinning of the current sheet in 10 min).

1. Introduction

The onset conditions for magnetospheric substorm are still poorly understood although the general contours are already well outlined [e.g., see, *Sergeev et al.*, 2012]. It is generally accepted that prior to an onset a current sheet has to be sufficiently thin (of the order of the proton inertial length) [*Shay et al.*, 1999], and the gradients of the plasma and magnetic field parameters have to be rather steep in order to lead to a development of the plasma instability [*Kivelson and Hughes*, 1990]. In many cases the instabilities may be related also to the presence of a magnetic field normal component minimum in the magnetotail [e.g., *Petrukovich et al.*, 2013]. Among the suggested instabilities there is the tearing mechanism [e.g., *Sitnov and Schindler*, 2010; *Zelenyi and Artemyev*, 2013], ballooning/interchange instability [e.g., *Raeder et al.*, 2010; *Pritchett and Coroniti*, 2013; *Panov et al.*, 2012a, 2012b], and double-gradient instability [*Erkaev et al.*, 2007; *Korovinskiy et al.*, 2013].

So far in most papers the current sheet stability analysis has been restricted to the symmetric geometry of the magnetotail, whereas in reality dipole is absolutely symmetric just in the separate moments of time, because it changes continuously. For the ~4 months (about 100 days) in a year the strict symmetry happens twice per day, and for the other 8 months the current sheet is always bent and shifted due to the nonzero dipole tilt. The asymmetry may cause generation of specific asymmetry-related instability modes (kink mode rather than sausage one) which grows faster. Therefore, breaking the symmetry of the magnetotail current sheet by introducing the dipole tilt or jumps of the solar wind parameters can make the physical conditions for the substorm onset more favorable. *Kivelson and Hughes* [1990] proposed that the increased field lines curvature in the bent current sheet will weaken the threshold for substorm onset. It means that exceptionally intense substorms with large *AL* magnitude can be mostly observed during periods of small tilt angles. This fact has later been demonstrated by statistical analysis [*Nowada et al.*, 2009]. The role of the fast changes of the solar wind flow direction as a potential factor of substorm activity has been recently pointed out [*Kubyshkina et al.*, 2011; *Panov et al.*, 2013; *Vörös et al.*, 2014].

In the present study we attempt to answer the question why the asymmetric factors are more efficient than the symmetric ones in triggering substorms, and we focus on the three main issues. First, we compare the effects of symmetric and asymmetric solar wind factors on the substorm occurrence rate to show that asymmetric impacts are more effective. Next, we present an extension to the Kan and Manankova solutions of the Vlasov equations for the tilted current sheet, which allows to analyze the stability of the asymmetric equilibrium. And, finally, we explore the penetration of the induced electric field, related to the current sheet bending,

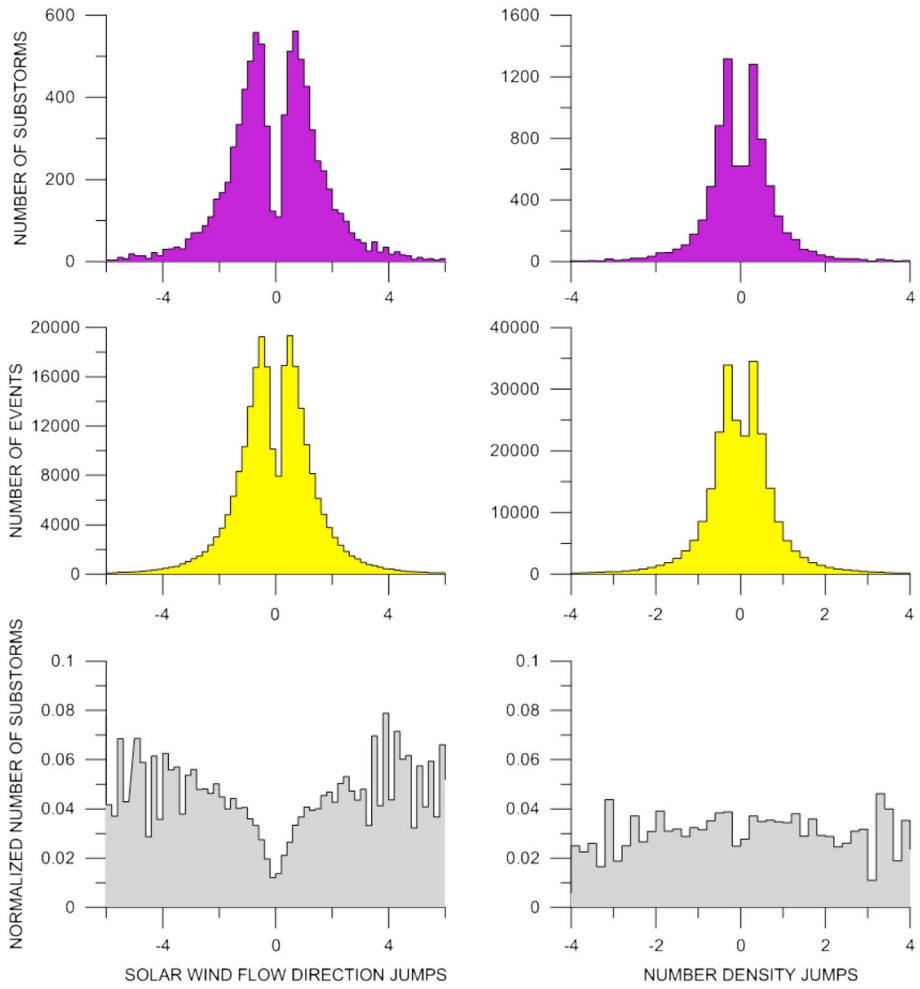

Figure 1. Distributions of the substorm occurrence during additional tilt due to (left column) solar wind flow rotations and (right column) solar wind number density enhancements. Shown are (top row) the substorm distributions themselves, (middle row) the normalization data (distributions of all 10 min intervals of tilt and density), and finally, (bottom row) the normalized distributions.

into the central part of the current sheet and the expected effects of this induced electric field on current sheet equilibrium.

2. Asymmetric Versus Symmetric Factors: Observations

The Earth's magnetotail is stretched along the solar wind flow, and fast changes in the solar wind velocity vector will produce rapid changes in current sheet configuration increasing or decreasing its asymmetry, bending, and shifting in (*XZ*) plane. We use the jumps of the solar wind flow direction as the asymmetric factor, which might be a trigger for the substorm activity. To quantify this factor we define the solar wind inclination angle against X_{GSM} axis as $\alpha = a\tan(V_z/V_x)$, where V_z and V_x are the solar wind velocity components. Later on we will talk about variations of this parameter ($\Delta\alpha$) as changes of the solar wind flow direction. We will then compare and contrast the number of substorms in our substorm onset list to the values of the solar wind flow direction jumps as described below.

For substorm onsets we use the database prepared by a method described in *Juusola et al.* [2011] and *Partamies et al.* [2013], where *AL* index curve was automatically analyzed and the substorm onset was defined as an abrupt decrease of at least 50 nT (which is the median absolute value of *AL* index during the whole data set) in the *AL* index (we did not actually select the isolated substorms). It should be noticed that we do not consider the substorm phases, so our study does not clearly relate to the growth phase duration or energy budget of substorm. These questions were investigated in detail in *Tanskanen et al.* [2002], for example.

The solar wind parameters (e.g., number density, solar wind magnetic field, and velocity components) were taken from the OMNI database.

From the data we know that the solar wind speed and velocity direction may change quite fast with characteristic period of about a minute, but the reaction of magnetosphere is not immediate and is estimated at approximately 10 min. Time lag of 10 min was chosen according to the two reasons. First, the mean distance which the solar wind pass in 10 min is about 30 R_E, and this distance corresponds to the area where we suppose to see the effect of the current sheet bending. Second, it is the time interval required by current sheet to thin twice under the effect of induced electric field (as will be shown in the next section).

We first calculated the maximum change of the solar wind direction (maximum $\Delta\alpha$) within 10 min before each onset for statistical analysis. After that we divide the angles from −6° to 6° into 120 bins and calculate the number of onsets corresponding to each bin (see Figure 1, top left). Angles larger than 6° were excluded because of the small number of events.

It is important to take into account that the occurrence rate of specific angles of solar wind inclination α is different. For normalization we take all 10 min intervals in the investigated period and calculate the maximum angle during each of these periods. We make a histogram with the same bins (Figure 1, middle left) and normalize the distribution of substorm number by it. The resulting normalized distribution is displayed in Figure 1 (bottom left).

One can see the deep minimum in the vicinity of the zero angle, which corresponds to the steady solar wind with an almost stable direction. The probability of the substorm occurrence increases with increasing solar wind inclination angle variation. In other words, the stronger the asymmetric factor (inclination angle of the solar wind velocity in our case), the higher the probability of the substorm activity. Probability for the maximum angles can be higher up to 6 times compared to the zero angle, but keeping in mind the errors, we expect the difference to be at least 2 times.

This result should be compared to that of the symmetric factor. To this end we use the jumps of the solar wind number density, i.e., the maximum change of density in 10 min intervals prior to onset.

It turned out that density jumps larger than 4 cm^{-3} are rare (less than 1.5% of events), and therefore, they were excluded from the list. Then we divided the density range from −4 to 4 cm^{-3} into 80 bins equal to 0.2 cm^{-3}. Finally, we normalized the substorm data set the same way as we did for the inclination angles. The result is presented in Figure 1 (bottom right).

After the normalization, the distribution of the substorm probability on density is uniform in contrast to the distribution of the inclination angle. Thus, we can see a dependence of substorm probability on the asymmetric parameter (inclination) rather than on symmetric one (density).

It is interesting to note that this result is not evident from the original distributions in Figure 1 (top row), where both of these distributions have a minimum at zero. Thus, the normalization is a necessary step to observe the effect.

One can see that errors are rather large for the solar wind flow direction jumps larger than |4°| (Figure 1, bottom row), since we obtain this plot as ratio of two small values from the tail of the distribution, shown in Figures 1 (top row) and 1 (middle row). But errors for the central interval (where the general effect appears) are much smaller, since number of events is large. As mentioned above, we use the OMNI database for solar wind data, which does not provide the possibility to obtain the errors directly. However, studies by *King and Papitashvili* [2005] and *Case and Wild* [2012] had proved that OMNI data are appropriate for the statistical analysis.

3. Asymmetric Current Sheet Equilibriums

The shape of the current sheet embedded in the plasma sheet in the near-Earth region is controlled by the dipole tilt angle and the direction of the solar wind [*Tsyganenko*, 2013]. A larger tilt gives more curved and more diverted (shifted in the Z direction from the equatorial plane) current sheet in the near-Earth region (~12 R_E). Unfortunately, it is not possible to use empirical Tsyganenko models for the stability analysis. Here we need a solution of the kinetic Vlasov equations corresponding to the current sheet equilibrium.

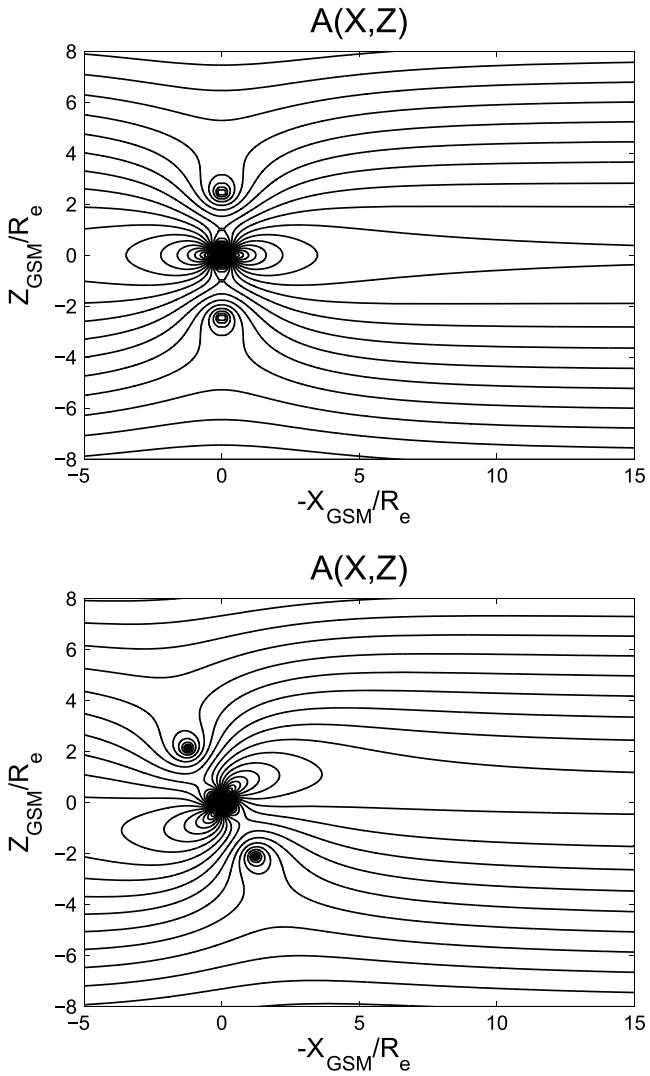

Figure 2. Magnetic field structure A(X,Z) = *const* of the generalized Kan model for the tilt angles equal to (top) 0° and (bottom) 30°.

We found a simple way to extend existing symmetric solutions in the case of a bent current sheet. We will illustrate the method for the relatively simple Kan solution [*Kan*, 1973], and the extension for more general Manankova equilibrium [*Manankova et al.*, 2000] follows straightforward.

The model by Kan is a special case of the Walker's solution [*Walker*, 1915] of the Grad-Shafranov equation, which is defined by the so-called generating function on complex variable $g(\zeta)$ following *Schindler* [1972] and *Yoon and Lui* [2005]:

$$e^{-2\Psi} = \frac{4|g'|^2}{(1+|g|^2)^2}, \quad g' = \frac{\partial g(\zeta)}{\partial \zeta}, \tag{1}$$

where $\zeta = X + iZ$ is a complex variable, Ψ is the magnetic potential, $B_x = -\frac{\partial \Psi}{\partial z}$, and $B_z = \frac{\partial \Psi}{\partial x}$. Specific solutions can be obtained by the choice of specific representation of g. For the symmetric Kan solution the generating function is

$$g(\zeta) = \exp[i\zeta - \frac{ib}{\zeta - a}], \tag{2}$$

and the configuration is defined by real parameters a and b. To obtain the asymmetric current sheet we have to make these parameters to be complex: $b \rightarrow be^{i\varphi}$, $a \rightarrow ia$, where φ is responsible for the dipole tilt, a controls

the shift of the current sheet in Z direction, and b is related to the elongation of the field lines. The magnetic potential for the asymmetric Kan solution can be presented in a relatively simple form

$$\Psi = \ln\left(\frac{ch[(z-a) - \frac{bx\sin(\varphi) - b(z-a)\cos(\varphi)}{x^2+(z-a)^2}]}{\sqrt{1 + \frac{2b\cos(\varphi)(x^2-(z-a)^2)+4x(z-a)b\sin(\varphi)+b^2}{(x^2+(z-a)^2)^2}}}\right). \quad (3)$$

The normalization was made according to *Yoon and Lui* [2005]; i.e., we introduce the characteristic magnetic field and distance

$$B_0^2 = 8\pi n_0(T_e + T_i), L = 2cT_i/(eB_0V_i),$$

where n_0 is the number density, T_e and T_i are electron and proton temperatures, respectively, and V_i is the proton drift speed. The magnetic potential Ψ is normalized to LB_0.

The asymmetric configuration in equation (3) contains the dipole singularity at (X,Z) = $(0, a)$ and two additional singularities at (X,Z) = $\left(\pm\sqrt{b}\sin\left(\frac{\varphi}{2}\right), \mp\sqrt{b}\cos\left(\frac{\varphi}{2}\right) + a\right)$, which rotate twice as slow as the dipole. This implies that it is the angle $\frac{\varphi}{2}$ which controls the current sheet bending. For the positive tilt angles the current sheet is bent and uplifted over the ecliptic plane, while for the negative tilt angles the current sheet is lifted down.

Configurations of magnetic field lines for the angles $\frac{\varphi}{2}$ equal to 0° and 30° are shown in Figure 2. The asymmetric solutions obtained here allow to analyze the stability of bent current sheet configurations.

4. Induced Electric Field

As the next step we study the quasi-dynamic modification of the Kan model. Although this model is static, we may allow the time dependence of the tilt angle. This way we obtain the time-depended current sheet configuration and can compute the induced electric field related to the changes of the current sheet bending as follows:

$$E_y(t) = -\frac{\partial\Psi}{\partial t} = -\frac{\partial\Psi}{\partial\varphi}\cdot\frac{\mathrm{d}\varphi}{\mathrm{d}t}, \quad (4)$$

where electric field is normalized to

$$E_0 = \frac{1}{c}\frac{B_0L}{T_0}. \quad (5)$$

Here T_0 is the characteristic time of the configuration changes. The variation of the magnetic field should be sufficiently slow, so that the inertial term $\rho\frac{\partial v}{\partial t}$ (ρ is the plasma density, v is the plasma velocity) becomes smaller than Amperé and pressure gradient forces. This means that the plasma speed has to be much smaller than Alfvén velocity. This condition is well fulfilled for the motion of plasma, caused by variations of the tilt angle and the solar wind direction jumps as used in our study.

To estimate the electric field produced by the current sheet reconfiguration under the dipole tilt changes, we take the following characteristic values: the magnetic field strength $B_0 = 20$ nT, thickness of the current layer $L = 2\ R_E$, and period of the dipole tilt variation $T_0 = 24$ h. As a result we obtain $E \sim 0.003$ mV m^{-1}. This weak electric field is probably unable to produce any noticeable dynamical effect. If we consider variations in the solar wind direction with a time period of 10 min, we get $E \sim 0.5$ mV m^{-1}, which is a significant value in terms of magnetotail dynamics.

In Figure 3 we present the distribution of the electric field produced by the changes in the solar wind inclination angle. The electric field is bipolar and has the opposite directions above and beneath the neutral plane. When the absolute value of the tilt angle grows, the electric field over the neutral plane becomes positive (directed along the current), while a decreasing tilt angle causes a negative (directed opposite to the current) electric field.

It is important that electric field penetrates to the center of the current sheet during a period of a sufficiently large tilt (Figures 3, top and 3, bottom). For small tilt angles (Figures 3, middle) $E \sim 0$ in this region. This electric

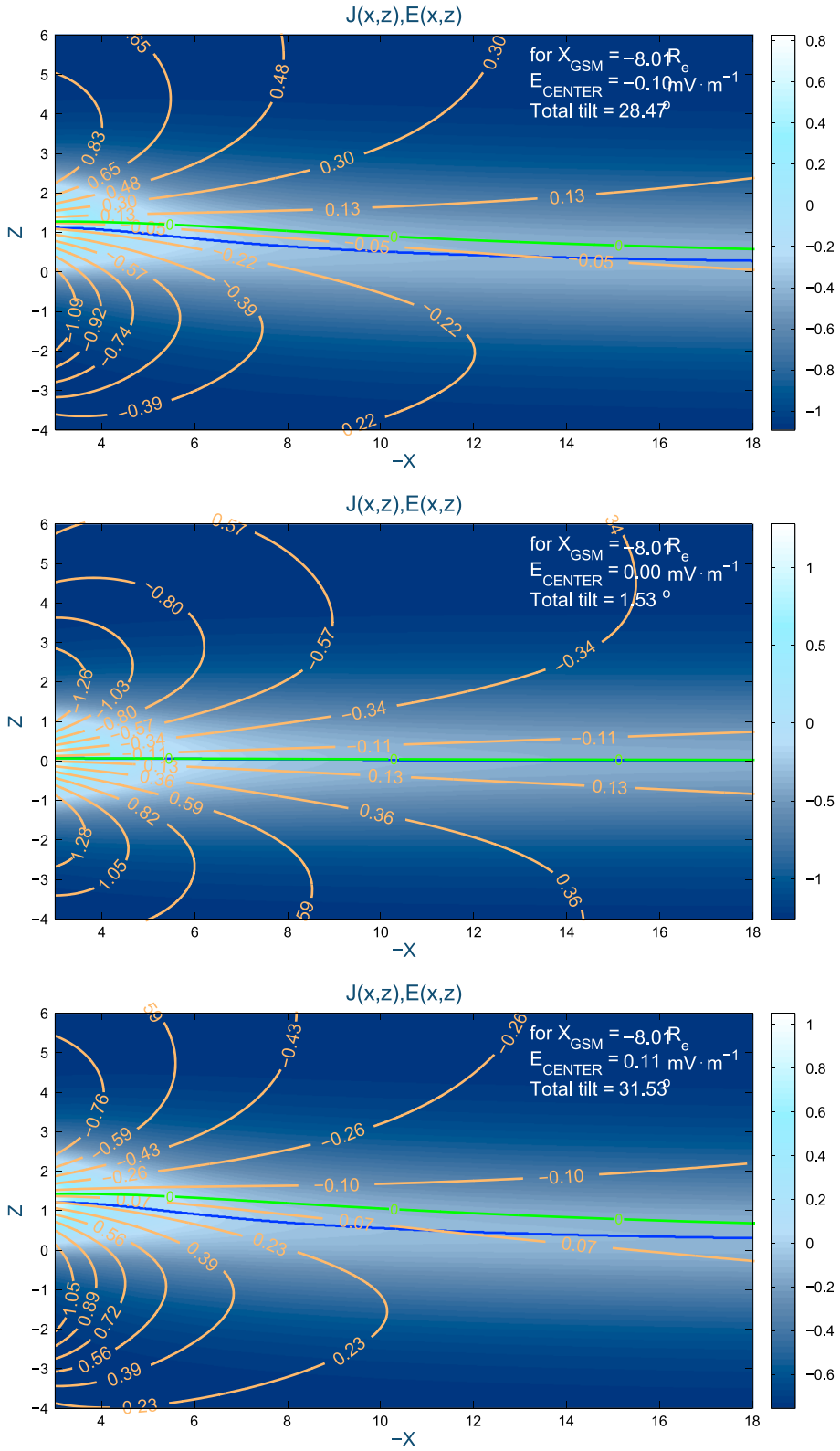

Figure 3. The distribution of the induced electric field. The current density is shown by the gray-blue color, electric field isolines are shown with the orange lines and the electric field zero line is shown with the green line. The numbers at the lines show the values of the electric field. (top) The initial tilt angle 30° is decreasing with the rate 4° per 10 min. (middle) The initial angle 0° increasing with the rate 4° per 10 min. (bottom) The initial angle 30° increasing with the rate 4° per 10 min.

field forces plasma to drift to the center of the current sheet (Figures 3, bottom, increasing total tilt angle), thinning the current sheet and creating conditions favorable for reconnection. If the tilt angle is decreasing (Figures 3, top) the penetrating electric field is negative, plasma drifts outward from the center of the current sheet, leading to the formation of a thicker current sheet. These conditions are known to be unlikely for reconnection.

The effect produced by the induced electric field depends on two separate factors. First, the value of the tilt angle defines the relative position of the current sheet center and electric field zero line (blue and green lines in Figure 3, respectively). For small tilt angles (less than 10°) these lines are almost fit and the entire current sheet moves up/down. For the big tilt angles (larger than 20°) nonzero-induced electric field penetrates the center of the current sheet and may provide the sheet thinning. Second, the specific value of the induced electric field depends on the jumps of the solar wind direction (its value and time scale). For the parameter α of 4°, the time of the direction change should be less than 15 min (for the bigger time electric field becomes less than 0.25 mV m^{-1} at the distance $-X \sim 10\ R_E$).

In the SI units the drift velocity value may be obtained as $\mathbf{V_{dr}} = [\mathbf{E}\times\mathbf{B}]/B^2$ and take the electric field to be equal to the induced electric field in the center of the current sheet, and magnetic field is equal to the magnetic field at the border of the current sheet (here we treat the line where the current density reduces in e times as the border). For the parameters used in the presented study (parameter $b = 1.5$ which corresponds to the initial sheet thickness of 2 R_E) at distance $-X \sim 10\ R_E$ plasma sheet thins twice in ~10 min.1).

5. Discussions and Results

The asymmetric nature of the solar wind-magnetosphere interaction can affect the magnetospheric dynamics in two different ways. First, it may cause direct dynamical changes in the magnetotail due to the appearance of induced electric field. As we showed the magnetotail variations related to the dipole tilt are too slow to generate observable effects; hence, only fast jumps of the solar wind direction or similar rapid variations of other parameters may change the tail dynamics. Second, a threshold of a plasma instability, which immediately causes a substorm, depends on the tilt angle. Though the origin of this instability is still unknown, we believe that current sheet bending is one of the major processes, which lowers the instability threshold. Thus, the investigations of the substorm onset definitely requires the stability analysis of the bent current sheet equilibrium. We left this problem for the future studies.

The main results of our study can be summarized as follows:

1. The asymmetric factors in the solar wind such as jumps of the solar wind flow direction are more effective in controlling the substorm activity than the symmetric ones, like pressure pulses or jumps of number density in the solar wind.
2. We obtained the extension of the existing solutions of the Grad-Shafranov equation (and also the 2D Vlasov equations) for the bent and shifted (in Z direction) current sheet by considering the control parameters of the Kan/Manankova models as complex values.
3. The rapid jumps of the solar wind direction generate induced electric field due to bending of the magnetotail. For large dipole tilt values this electric field penetrates to the center of the current sheet and causes its thinning. This is true when a solar wind change induced additional tilt acts in the direction to increase the bending of the current sheet. Otherwise, if the additional tilt decreases the bending, it leads to a thicker current sheet. This effect is small for the initial zero (or small) dipole tilt values.

Our results support the idea that breaking the symmetry of the current sheet provides favorable conditions for substorm triggering. This implies that the symmetric current sheet is more effective in accumulating the magnetic flux, and the reconnection can then produce more intense substorm with larger $|AL|$ index. The well bent current sheet seems to have lower threshold for the reconnection, and therefore, the resulting substorms are less intense (smaller $|AL|$ index values) but more often.

Acknowledgments
This study has been supported by Russian Science Foundation grant 1417-00072. *AE* and *Dst* index data are downloaded from the World Data Center for Geomagnetism in Kyoto at http://wdc.kugi.kyoto-u.ac.jp. The southern *AE* index data were downloaded from the virtual magnetic observatory at vmi.gsfc.nasa.gov as prepared by UCLA. Solar wind and interplanetary magnetic field data were downloaded from OMNI Web at http://omniweb.gsfc.nasa.gov/.

The Editor thanks Tuija Pukkinen and an anonymous reviewer for their assistance in evaluating this paper.

References

Case, N. A., and J. A. Wild (2012), A statistical comparison of solar wind propagation delays derived from multispacecraft techniques, *J. Geophys. Res.*, *117*, A02101, doi:10.1029/2011JA016946.

Erkaev, N. V., V. S. Semenov, and H. K. Biernat (2007), Magnetic double-gradient instability and flapping waves in a current sheet, *Phys. Rev. Lett.*, *99*(23), 235003, doi:10.1103/PhysRevLett.99.235003.

Juusola, L., N. Østgaard, E. Tanskanen, N. Partamies, and K. Snekvik (2011), Earthward plasma sheet flows during substorm phases, *J. Geophys. Res.*, *116*, A10228, doi:10.1029/2011JA016852.

Kan, J. R. (1973), On the structure of the magnetotail current sheet, *J. Geophys. Res.*, *78*, 3773–3781.

King, J. H., and N. E. Papitashvili (2005), Solar wind spatial scales in and comparisons of hourly Wind and ACE plasma and magnetic field data, *J. Geophys. Res.*, *110*, A02104, doi:10.1029/2004JA010649.

Kivelson, M. G., and W. J. Hughes (1990), On the threshold for the triggering substorms, *Planet. Space Sci.*, *38*(2), 211–220.

Korovinskiy, D. B., A. Divin, N. V. Erkaev, V. V. Ivanova, I. B. Ivanov, V. S. Semenov, G. Lapenta, S. Markidis, H. K. Biernat, and M. Zellinger (2013), MHD modeling of the double-gradient (kink) magnetic instability, *J. Geophys. Res. Space Physics*, *118*, 1146–1158, doi:10.1002/jgra.50206.

Kubyshkina, M., V. Sergeev, N. Tsyganenko, V. Angelopoulos, A. Runov, E. Donovan, H. Singer, U. Auster, and W. Baumjohann (2011), Time-dependent magnetospheric configuration and breakup mapping during a substorm, *J. Geophys. Res.*, *116*, A00I27, doi:10.1029/2010JA015882.

Manankova, A. V., M. I. Pudovkin, and A. V. Runov (2000), Stationary configurations of the two-dimensional current-carrying plasma sheet: Exact solutions, *Geomag. Aeron.*, *40*, 430–438.

Nowada, M., J.-H. Shue, and C. T. Russel (2009), Effects of dipole tilt angle on geomagnetic activity, *Planet. Space Sci.*, *57*, 1254–1259.

Panov, E. V., V. A. Sergeev, P. L. Pritchett, F. V. Coroniti, R. Nakamura, W. Baumjohann, V. Angelopoulos, H. U. Auster, and J. P. McFadden (2012a), Observations of kinetic ballooning/interchange instability signatures in the magnetotail, *Geophys. Res. Lett.*, *39*, L08110, doi:10.1029/2012GL051668.

Panov, E. V., et al. (2012b), Kinetic ballooning/interchange instability in a bent plasma sheet, *J. Geophys. Res.*, *117*, A06228, doi:10.1029/2011JA017496.

Panov, E. V., M. V. Kubyshkina, R. Nakamura, W. Baumjohann, V. Angelopoulos, V. A. Sergeev, and A. A. Petrukovich (2013), Oscillatory flow braking in the magnetotail: THEMIS statistics, *Geophys. Res. Lett.*, *40*, 2505–2510, doi:10.1002/grl.50407.

Partamies, N., L. Juusola, E. Tanskanen, and K. Kauristie (2013), Statistical properties of substorms during different storm and solar cycle phases, *Ann. Geophys.*, *31*, 349–358, doi:10.5194/angeo-31-349-2013.

Petrukovich, A. A., A. V. Artemyev, R. Nakamura, W. Baumjohann, and E. V. Panov (2013), Cluster observations of $\partial B_z/\partial x$ during growth phase magnetotail stretching intervals, *J. Geophys. Res. Space Physics*, *118*, 5720–5730, doi:10.1002/jgra.50550.

Pritchett, P. L., and F. V. Coroniti (2013), Structure and consequences of the kinetic ballooning/interchange instability in the magnetotail, *J. Geophys. Res. Space Physics*, *118*, 146–159, doi:10.1029/2012JA018143.

Raeder, J., P. Zhu, Y. Ge, and G. Siscoe (2010), Open geospace general circulation model simulation of a substorm: Axial tail instability and ballooning mode preceding substorm onset, *J. Geophys. Res.*, *115*, A00I16, doi:10.1029/2010JA015876.

Schindler, K. (1972), A self-consistent theory of the tail of the magnetosphere, in *Earth's Magnetospheric Processes*, edited by B. M. McComas, pp. 200, D. Reidel, Norwell, Mass.

Sergeev, V. A., V. Angelopoulos, and R. Nakamura (2012), Recent advances in understanding substorm dynamics, *Geophys. Res. Lett.*, *39*, L05101, doi:10.1029/2012GL050859.

Shay, M. A., J. F. Drake, B. N. Rogers, and R. E. Denton (1999), The scaling of collisionless, magnetic reconnection for large systems, *Geophys. Res. Lett.*, *26*, 2163–2166.

Sitnov, M. I., and K. Schindler (2010), Tearing stability of a multiscale magnetotail current sheet, *Geophys. Res. Lett.*, *37*, L08102, doi:10.1029/2010GL042961.

Tanskanen, E., T. I. Pulkkinen, H. E. J. Koskinen, and J. A. Slavin (2002), Substorm energy budget during low and high solar activity: 1997 and 1999 compared, *J. Geophys. Res.*, *107*(A6), 1086, doi:10.1029/2001JA900153.

Tsyganenko, N. A. (2013), Data-based modelling of the Earth's dynamic magnetosphere: A review, *Ann. Geophys.*, *31*(10), 1745–1772, doi:10.5194/angeo-31-1745-2013.

Vörös, Z., G. Faskó, M. Khodanchenko, I. Honkonen, P. Janhunen, and M. Palmroth (2014), Windsock memory COnditioned RAM (CO-RAM) pressure effect: Forced reconnection in the Earth's magnetotail, *J. Geophys. Res. Space Physics*, *119*, 6273–6293, doi:10.1002/2014JA019857.

Walker, G. W. (1915), Some problems illustrating the forms of nebulae, *Proc. R. Soc. London, Ser. A*, *91*, 410–420.

Yoon, P. H., and A. T. Y. Lui (2005), A class of exact two-dimensional kinetic current sheet equilibria, *J. Geophys. Res.*, *110*, A01202, doi:10.1029/2003JA010308.

Zelenyi, L., and A. Artemyev (2013), Mechanisms of spontaneous reconnection: From magnetospheric to fusion plasma, *Space Sci. Rev.*, *178*, 441–457, doi:10.1007/s11214-013-9959-8.